

See discussions, stats, and author profiles for this publication at: <https://www.researchgate.net/publication/263955062>

Synthesis of Magnetic Cobalt Nanoparticles Anchored on Graphene Nanosheets and Catalytic Decomposition of Orange II

ARTICLE in INDUSTRIAL & ENGINEERING CHEMISTRY RESEARCH · NOVEMBER 2013

Impact Factor: 2.59 · DOI: 10.1021/ie401690h

CITATIONS

22

READS

125

6 AUTHORS, INCLUDING:



[Yunjin Yao](#)

Hefei University of Technology

25 PUBLICATIONS 804 CITATIONS

[SEE PROFILE](#)



[Shaobin Wang](#)

Curtin University

271 PUBLICATIONS 9,327 CITATIONS

[SEE PROFILE](#)

Synthesis of Magnetic Cobalt Nanoparticles Anchored on Graphene Nanosheets and Catalytic Decomposition of Orange II

Yunjin Yao,^{*,†,‡,§} Chuan Xu,^{†,‡} Jiacheng Qin,^{†,‡} Fengyu Wei,^{†,‡} Mengnan Rao,^{†,‡} and Shaobin Wang^{*,§}

[†]School of Chemical Engineering, Hefei University of Technology, Hefei 230009, People's Republic of China

[‡]Anhui Key Laboratory of Controllable Chemical Reaction & Material Chemical Engineering, Hefei 230009, People's Republic of China

[§]Department of Chemical Engineering, Curtin University, G.P.O. Box U1987, Perth, Western Australia 6845, Australia

ABSTRACT: Magnetic cobalt nanoparticles (NPs) at a size of approximately 29.9 nm anchored on graphene sheets were prepared and tested for heterogeneous oxidation of a dyeing pollutant, Orange II, with peroxyomonosulfate (PMS) in aqueous solutions. The physicochemical properties of Co-graphene hybrids were investigated by various characterization techniques, such as powder X-ray diffraction (XRD), thermogravimetric analysis (TGA), field emission scanning electron microscopy (FESEM), transmission electron microscopy (TEM), energy-dispersive X-ray spectrometer (EDS), Raman spectroscopy, and X-ray photoelectron spectroscopy (XPS). The incorporation of Co NPs and graphene sheets produces much higher catalytic activity of Orange II degradation than pure Co. The Orange II decomposition rate increases with increasing temperature (25–45 °C), pH (4–10), and PMS dosage (0.04–0.60 g/L) but decreases with its increased concentration (30–120 mg/L). Kinetic studies show decomposition of Orange II on Co-graphene can be described by a pseudo-first-order kinetic model with activation energy of 49.5 kJ/mol.

1. INTRODUCTION

In recent years, advanced oxidation processes (AOPs) such as catalytic wet air oxidation, catalytic wet peroxide oxidation, catalytic ozonation, and photocatalysis using various oxidants such as hydrogen peroxide, O₂, O₃, persulfate, and peroxyomonosulfate are becoming more and more important technologies for water decontamination.¹ By activation of various transition metals in different forms, such as Fe^o, Fe(II), or Fe oxides, these oxidants can produce free radicals that are more powerful in degrading organic contaminants in aqueous solutions than the parent oxidants. Among these AOPs, ·OH from H₂O₂ is the main reactive and oxidizing radical to degrade organic contaminants. However, the ·OH oxidation process suffers from drawbacks such as the high cost in the production, transport, and storage of H₂O₂, as well as pH adjustments.²

Recently, the oxidation of organic compounds by a sulfate oxidant, peroxyomonosulfate (PMS), has been studied in AOPs because PMS could produce sulfate radicals (SO₄^{·-}) by radiolytic, photolytic, and thermal activation and transition metals. It has been discovered that SO₄^{·-} is more powerful than ·OH and that SO₄^{·-} in general is more selective for oxidation than ·OH.^{3,4} Many studies in the PMS activation have focused on cobalt ions and supported cobalt oxide catalysts because of their best activation efficiency.^{5,6} Nevertheless, Co(II) is a highly toxic ion and can bring out several health problems for drinking water.^{5,7} Based on all these studies, despite some promising outcomes on improving the catalytic activity, it is still a great challenge to make the heterogeneous PMS activation technology commercially feasible.

The magnetic particle technology has been receiving considerable attention in recent years for its benefits in solving environmental problems.⁸ Magnetic particles can be easily separated from a medium using a simple magnetic process. As

is well-known, magnetic cobalt nanoparticles (NPs) are good candidates for potential applications in catalysis and information storage.^{9,10} Although Co NPs could present high catalytic performance, they showed poor chemical and thermal stabilities as well as displaying particle aggregation, leading to lower catalytic efficiency in long-term application. The development of active and stable heterogeneous Co-based catalysts for water treatment is important, and varying approaches using different supports (e.g., clays, carbon materials, zeolites) have been reported.¹¹

Compared to other carbon allotropes such as graphite, carbon black, diamond, and carbon nanotubes, graphene exhibits a structure of 2D sheets composed of sp²-bonded carbon atoms with one or more atomic thicknesses and has unique physical properties such as high surface area, superior electric conductivity, excellent mechanical strength, and elasticity.^{12–15} Graphene has been explored as either a metal-free catalyst through molecular engineering or a unique support for metal-based catalysts. Studies on graphene–metal interactions reveal that charge transfers can occur across the graphene–metal interface. Such a charge transfer may be the main contributor to the enhanced catalytic activities on certain NPs supported on graphene catalysts such as Co₃O₄–graphene,^{16,17} Co(OH)₂–graphene,¹⁸ MnCo₂O₄–graphene,¹⁹ and Co/CoO–graphene.²⁰ Co-graphene hybrid materials have been recently prepared as anode and supercapacitor materials with performance comparable to that of previously reported Co-based anodes.²⁰ Previously, we prepared magnetic Fe₃O₄–

Received: May 27, 2013

Revised: October 31, 2013

Accepted: November 18, 2013

Published: November 18, 2013

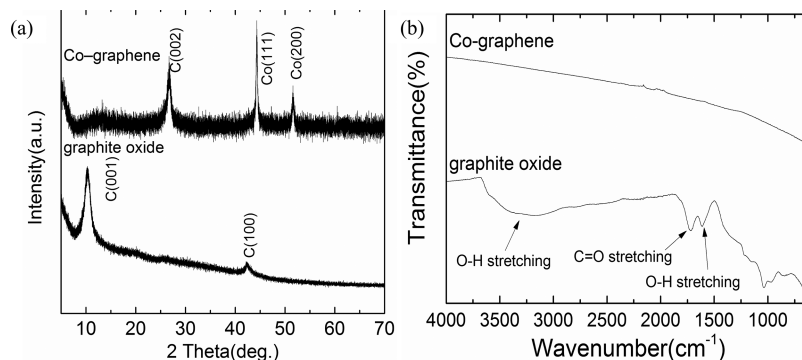


Figure 1. XRD patterns (a) and FTIR spectra (b) for graphite oxide and Co-graphene hybrid.

graphene,¹³ Fe₃O₄@SiO₂–graphene,²¹ and CoFe₂O₄–graphene²² for the degradation of organic pollutants in water. However, little work has been done in magnetic Co–graphene hybrids for catalytic reactions, in particular, for the heterogeneous activation of PMS for organic oxidation.

Here, we report a facile approach for magnetic Co–graphene preparation and its performance in catalytic degradation of Orange II by PMS. The physical and chemical properties of Co–graphene hybrids were determined using various techniques, and the catalytic behavior in heterogeneous reaction using different oxidants (H₂O₂, persulfate, and PMS) was evaluated. The effects of the reaction conditions (e.g., pH, Orange II and PMS concentration, and temperature) on catalytic activity, reaction kinetics and degradation mechanism, were comprehensively studied.

2. MATERIALS AND METHODS

2.1. Synthesis of Co–Graphene Hybrids. Graphite oxide was synthesized from natural graphite by the modified Hummers method as described elsewhere.^{21,23,24} For preparation of Co–graphene hybrids, 0.5 g of graphite oxide was dispersed in the solution under ultrasonic conditions for 2 h to achieve uniform dispersion of graphene oxide (GO), and 0.4932 g of Co(NO₃)₂·6H₂O was dissolved in 20 mL of distilled water under magnetic stirring. Then, Co(NO₃)₂·6H₂O aqueous solution was added into the GO dispersion under vigorous magnetic stirring for 1 h, and 20 mL of 28% concentrated ammonia aqueous solution were added slowly to the above mixture to make a solution with pH > 10, followed by 4 h stirring. After that, 10 mL of hydrazine hydrate was added to the above solution, and then the solution temperature was raised to 80 °C with constant stirring, resulting in a black solution. After 5 h of stirring, the solution was cooled to room temperature naturally, and the precipitates were obtained by centrifugation separation, washed with distilled water and absolute ethanol, and then dried under a vacuum. Finally, after annealing at 500 °C for 2 h under Ar/H₂ (4:1 v/v) gas flow, Co–graphene hybrids were successfully fabricated. For a comparison, bare graphene was also prepared as in the above procedure but without adding Co(NO₃)₂·6H₂O and annealing with high temperature.^{25,26} All the products were stored in a desiccator for further experiments.

2.2. Catalyst Characterization. The structure of all samples was characterized by powder X-ray diffraction (XRD) with a Bruker Advance D-8 diffractometer using Cu K α ($\lambda = 1.5418 \text{ \AA}$) radiation at a voltage of 40 kV and a generator current of 40 mA with a scanning speed of 5°/min from 5 to 70°. FTIR spectra were recorded on a Perkin-Elmer Spectrum

100 with a resolution of 4 cm⁻¹ in transmission mode at room temperature. Raman measurements were carried out on a Dilor Labram model 1B dispersive Raman spectrometer using the helium–neon laser at 632.8 nm. X-ray photoelectron spectroscopy (XPS) analysis was performed on an ESCALAB250 spectrometer equipped with a monochromatized Al K α source analyzer to characterize the particles' surface. The morphology and microstructure of samples were analyzed by field emission scanning electron microscopy (FESEM) (Zeiss Neon 40EsB FIBSEM) and transmission electron microscopy (TEM) (JEOL 2011 TEM) equipped with an energy-dispersive X-ray spectrometer (EDS). For TEM, a suspension of Co–graphene hybrids in ethanol was dropped onto a copper grid covered with carbon film. Thermogravimetric analysis (TGA) and differential thermal analysis (DTA) of samples were determined on a Perkin-Elmer Diamond TG/DTA thermal analyzer in air flow or argon flow with a heating rate of 5 °C/min at a gas rate of 100 mL/min.

2.3. Catalyst Evaluation. The catalytic reactions were carried out in a 500 mL glass beaker with a magnetic stirrer, a heating jacket, and a condenser. An aliquot of stock solution of Orange II (or other substrate, 600 mg/L) was added to make a desired concentration (typically 60 mg/L), and then the reaction was initiated by the sequential addition of a catalyst and Oxone. Unless otherwise mentioned, catalyst loading in solution was fixed at 0.01 g/L. The initial pH of the solution was adjusted to a desired value with 1 N NaOH and HNO₃ standard solutions. The reactions were carried out for various times, and sample aliquots (1 mL) were withdrawn at regular time intervals from the reactor and injected into 4 mL glass vials containing 1 mL of methanol to quench residual radical SO₄[•]. All experiments were carried out in triplicate at the given conditions. The temporal concentration of dye in withdrawn water samples was analyzed by UV-vis spectrophotometry at the maximum absorption band (484 nm). The reaction was also carried out at different temperatures (25, 35, and 45 °C). Orange II degradation was tested at four initial concentrations from 30 to 120 mg/L. Four different catalysts, pure Co and Co₃O₄ NPs, Co²⁺ ions, and Co–graphene, were used. Oxone was also tested at several doses from 0.04 to 0.60 mg/L. A few other tests were carried out with different oxidants, such as H₂O₂ and K₂S₂O₈ (PS). For selected samples, total organic content (TOC) was determined using an IL550 TOC-TN analyzer. Before measuring TOC, 5 mL of sample were extracted and quenched with 5 mL of 3 M sodium nitrile solution. The measurements of Co ion concentration in reacted solutions were also made using an atomic absorption spectroscopy (AAS, AA800, Perkin-Elmer).

3. RESULTS AND DISCUSSION

3.1. Catalyst Characterization. XRD patterns and FTIR spectra of graphite oxide and Co-graphene hybrid are shown in Figure 1. The original graphite oxide shows a sharp peak at $2\theta = 10.3^\circ$ corresponding to the (001) reflection of graphite oxide, indicating a well-ordered layered structure. However, the characteristic peak of graphite oxide cannot be observed in the XRD pattern of Co-graphene hybrid, suggesting graphite oxide was effectively exfoliated. Meanwhile two diffraction peaks at $2\theta = 44.35^\circ$ and 51.64° for Co-graphene hybrid appeared and can be indexed to the (111) and (200) reflections of face-centered cubic (fcc) metallic cobalt (JCPDS 15-0806), respectively, confirming that the cobalt precursor has been chemically reduced to Co NPs by H_2 , which is the same as previous reports.²⁷ A broad diffraction peak (002) on Co-graphene appears at a 2θ of 26.73° , which can be indexed to the graphene sheets.²⁸ The diffraction peak for Co (111) was used to estimate the Co crystallite size. An average crystallite size of about 29.9 nm for Co NPs was calculated by using the Debye-Scherrer formula,^{21,29} which is consistent with the TEM results (see Figure 4). The FTIR spectra from the Co-graphene hybrid (Figure 1b) and pristine graphite oxide indicate removal of functional groups from graphite oxide under the reaction conditions employed for synthesis.³⁰

Figure 2 presents Raman spectra of bare graphene and Co-graphene hybrid. The G band ($\sim 1595 \text{ cm}^{-1}$) referring to sp^2 -

not only O 1s and C 1s peaks but also peaks at 799.4 and 779.5 eV corresponding to the Co 2p_{1/2} and Co 2p_{3/2} states, confirming the presence of Co species in the hybrids (Figure 3a,c). The reduced graphene (Figure 3a,b) obtained after H_2 reduction shows remarkably reduced contribution of the C 1s components associated with oxygenated functional groups compared with that of graphite oxide, suggesting deoxygenation of graphene oxide occurred in the reduction reaction.³³ However, residual oxygen functional groups on graphene could still capture metal ions for in situ synthesis of metal NPs on graphene. A small chemical shift toward higher binding energies occurred for Co2p_{3/2} (779.5 eV) and Co2p_{1/2} (799.4 eV) (Figure 3c) as compared to those of metallic Co (Co 2p_{3/2} (778.10 eV) and Co 2p_{1/2} (793.30 eV)), implying that the Co on the surface of the graphene sheets is being oxidized. The GO reduction and restoration of the conjugated aromatic system result in good electronic conductivity, making a good electron transfer on graphene surface.³⁴

For further insights into the morphology and structure of hybrid Co-graphene nanosheets, FESEM and TEM investigations were carried out (Figure 4). Low-magnification SEM (Figure 4c) and TEM images (Figure 4a,b) show that cobalt particles have decorated on both sides of the graphene nanosheets with a narrow size distribution and uniform dispersion. The magnified TEM image (Figure 4b) displays that the typical cobalt particle size is in the range of 15–45 nm (average: 30 nm) (inset of Figure 4b), which is similar to the average particle size from XRD pattern (29.9 nm). It should be noted that even after a long time of sonication during the fabrication of the TEM specimen, there are very few cobalt NPs in the region of copper grid where graphene sheets are absent, indicating the strong interaction between the Co NPs and graphene sheets. The low aggregation of Co NPs indicates that the graphene nanosheets could make good dispersion of the Co NPs. Based on the TEM images, an intimate interaction between the Co NPs and the graphene sheets occurs, and such a combination will produce fast electron transport through the graphene matrix to the Co NPs, leading to efficient chemical performance.³⁵ As seen, both the TEM and SEM images indicate the formation of thin graphene sheets.³⁶ EDS as shown in Figure 4d further confirmed the formation of Co-graphene hybrid. The EDS spectrum shows the peaks of C, O, and Co elements on the hybrid, whereas Cu and Si peaks are attributed to the TEM grid, confirming the deposition of Co NPs on graphene sheets.

The thermal stability of Co-graphene hybrids has been measured by TG-DTA under air or argon flow. It was shown in Figure 5 that about 3.0% weight enhancement occurred between 220 and 380 °C, and meanwhile, a broad exothermic peak appeared on the DTA curve, which was attributed to the oxidation of Co to Co_3O_4 by air flow.³⁷ In addition, a subsequent weight loss attributed to the rapid combustion of the graphene shells. At the temperature of 460–630 °C, a strong exothermic peak (530 °C) was observed in the DTA curve. In contrast, in argon flow, Co-graphene hybrid shows strong thermal stability with a gradual weight loss (< 8%) up to 900 °C, and no abrupt exothermal peak occurred. This is consistent with the thermal behavior of graphene itself in an argon atmosphere as reported before.³⁸ The total mass loss of 62% of the hybrids during the oxidation process suggests that the weight content of the Co NPs in the Co-graphene hybrids should be approximately 28%, on the basis of the assumption

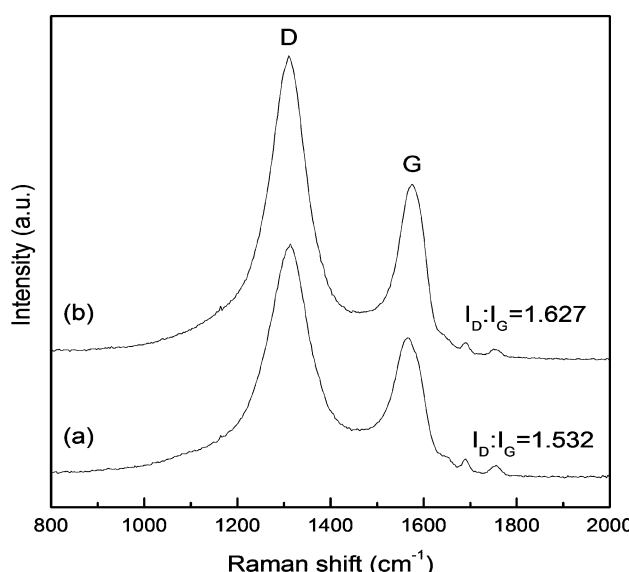


Figure 2. Raman spectra of (a) graphene and (b) Co-graphene.

hybridized carbon and the D band ($\sim 1352 \text{ cm}^{-1}$) relating to disordered carbon are appearing on both samples. The D to the G band intensity ratio (I_D/I_G) suggests the disorder extent and crystallite size of the graphitic layers. The intensity ratio (1.53) of I_D/I_G for graphene is closer to that (1.63) of Co-graphene hybrid, suggesting that there is a reduction of exfoliated GO. These results confirm the existence of graphene in the as-prepared hybrids.³¹

The surface chemical compositions and the valence states of samples were determined by XPS. For the graphene sample (Figure 3a), the main peak centered at about 284.6 eV is originated from the graphitic sp^2 carbon atoms.³² Compared to graphene, XPS spectrum of the Co-graphene hybrid exhibits

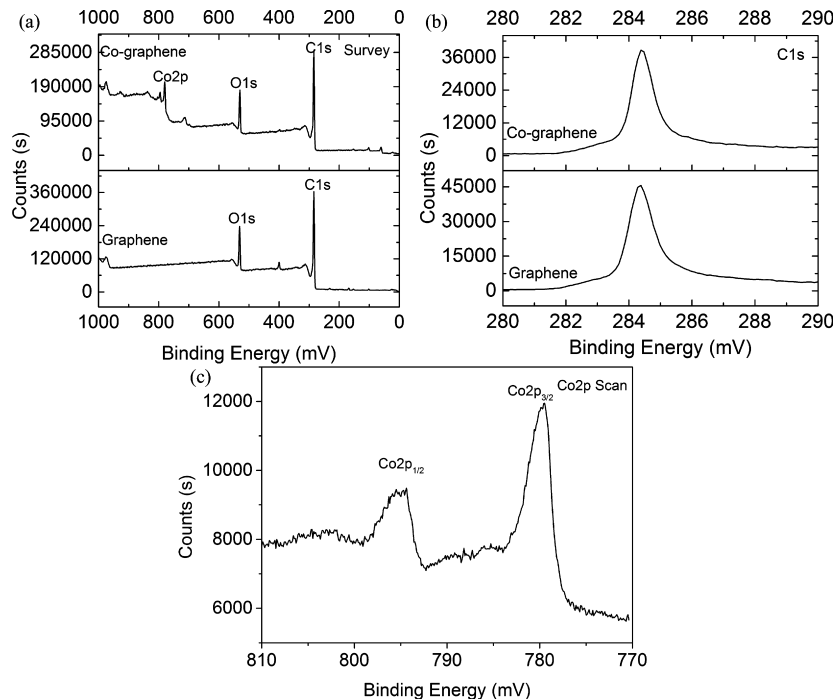


Figure 3. XPS spectra of graphene and Co-graphene: (a) survey scan; (b) C 1s region; (c) Co 2p region.

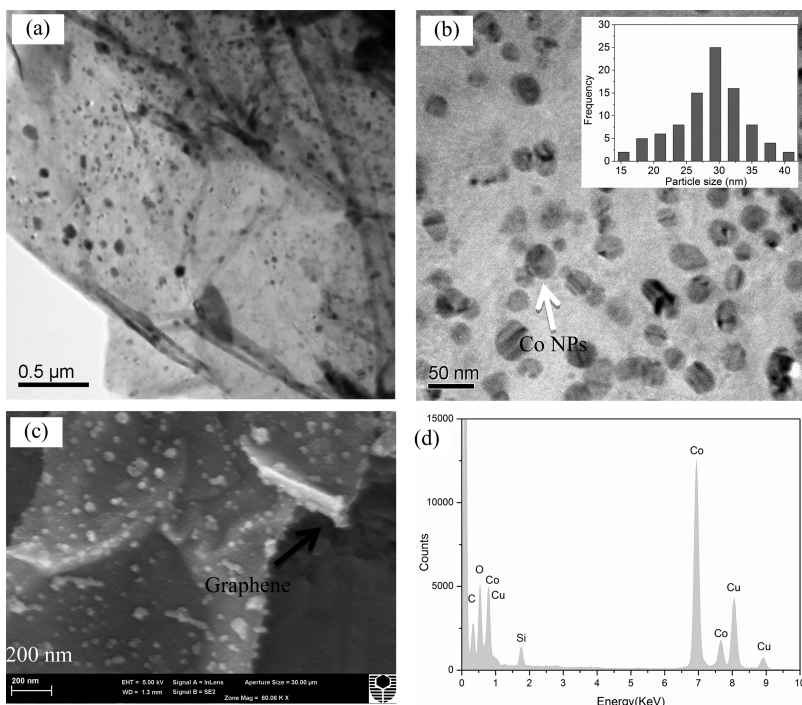


Figure 4. (a–b) TEM images with different magnifications of Co-graphene hybrid. (c) SEM image of Co-graphene hybrid. (d) EDS of the hybrid. Inset figure shows the particle size distribution.

that all Co has transferred to Co_3O_4 and all C has been burnt out.

As stated in the Introduction, the magnetic properties of Co NPs give a good performance in magnetic separation for the Co-graphene catalysts. As shown in Figure 6, when a magnet approaches the dispersion of water at room temperature, Co-graphene particles are attracted to the sidewall of the magnet in 20 s, and the solution becomes clear and transparent. It demonstrates that, in an external magnetic field, Co-graphene

particles can be magnetized and enriched because of their strong paramagnetic property. When the magnetic field is removed, the magnetization decays rapidly to zero, and Co-graphene particles will be redispersed in aqueous solution.

3.2. Catalytic Evaluation. Orange II, as one of the important organic dyes, has been widely used in textile industry, which often contaminates the environment.^{39,40} Figure 7 presents the degradation of Orange II using different oxidants (PMS, PS, and H_2O_2) for generating active radicals by Co-

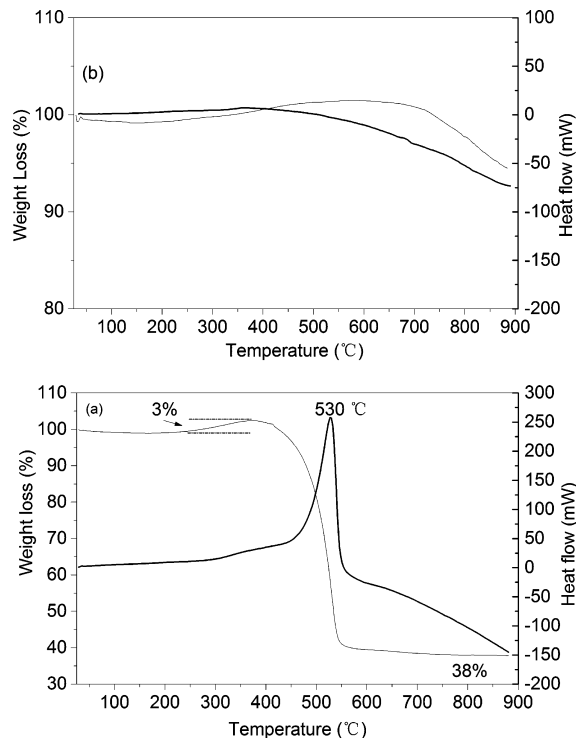


Figure 5. TG-DTA curves of Co-graphene in an air flow (a) and an argon flow (b) atmosphere.

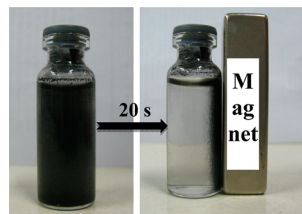


Figure 6. Photograph representing the magnetic enrichment of the Co-graphene suspension.

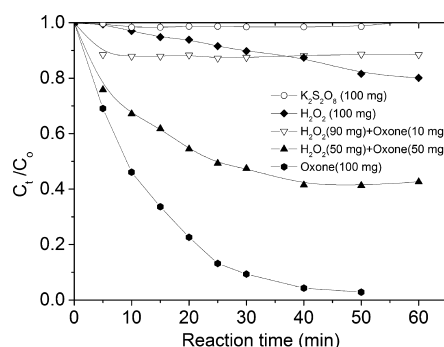


Figure 7. Effect of the different oxidants on degradation efficiency by the Co-graphene hybrids. Reaction conditions: [Orange II] = 60 mg/L, [Co-graphene] = 0.01 g/L, pH = 7, T = 25 °C.

graphene hybrids. The order of the degradation efficiencies is Co-graphene/PMS > Co-graphene/H₂O₂ > Co-graphene/PS. Co-graphene with H₂O₂ and PS would produce less than 10% degradation of dye in 1 h, indicating that Co-graphene is not effective in activation of H₂O₂ and PS to produce ·OH and SO₄[•] radicals, respectively. The performance with PMS, however, was much better than that of PS and H₂O₂ because

of a strong reaction of PMS with Co-graphene to generate SO₄[•]. It is known that PMS has a higher oxidizing potential than H₂O₂ and that the PMS molecule is not symmetric, with only one H replaced by SO₃. Thus, PMS might be more easily activated than the other two oxidants.⁴¹ Anipsitakis and Dionysiou⁴² have reported slow reaction rates for Co²⁺/H₂O₂ and Co²⁺/PS in homogeneous systems. Similarly, a slower reaction rate in heterogeneous systems would also occur in this investigation.

Catalytic activities of Co-graphene hybrid compared with other materials in homogeneous or heterogeneous activation of PMS for the oxidation of Orange II are shown in Figure 8a. Under reaction conditions, Orange II solution gradually degraded within 1 h upon SO₄[•] in the presence of Co-graphene hybrid, indicating that the chromophoric structure of the dye was destroyed during the period. However, the catalytic activities of pure Co and Co₃O₄ were much lower. For pure Co sample, Orange II was removed at 88%, whereas for pure Co₃O₄, 31% of Orange II were degraded at 60 min. Under the tested conditions, Orange II degradation seemed to follow pseudo-first-order reaction in kinetics, which is expressed as $\ln(C_t/C_0) = -k_{\text{obs}}t$, where t is reaction time (min), k_{obs} is the apparent rate constant (min⁻¹), and C_0 and C_t are pollutant concentrations (mg/L) at time of $t = 0$ and $t = t$, respectively. It was seen that the degradation rates using different catalysts under the same operation decreased in the following order: Co²⁺/PMS > Co-graphene/PMS > Co/PS > Co₃O₄/PS. Thus, the magnetic cobalt on graphene is active as close to the homogeneous Co²⁺ ions. They are also superior to the unsupported Co₃O₄ catalyst. The combination of Co and graphene produces a synergistic effect in catalytic activity, leading to enhanced relative rates of mass transfer to and chemical reaction at reactive sites, similar to that of Co₃O₄-graphene¹⁷ and CoFe₂O₄-graphene²² catalysts.

The solutions using Co-graphene catalyst after reaction were collected. TOC and concentrations of leached Co ions in the solutions were analyzed. TOC removal was 20% less than the corresponding extent of Orange II removal, implying the presence of reaction intermediates in the solution. The Co concentration was detected to be 0.10 mg/L, which was contributed to leached Co from Co-graphene catalyst. As a comparison, homogeneous catalysis by Co ion was further determined in the same reaction system, as shown in Figure 8. Compared to the activity of supported catalysts, Co leaching has a minor contribution to the activity in activation of PMS. In addition, the performance of Co-graphene catalyst in a second run of used catalysts has also been tested (Figure 8). The efficiencies remained very high, though a little decrease in Orange II removal efficiencies was observed, which may be ascribed to cobalt leaching, coverage of intermediates, and change in surface charges of the Co-graphene catalyst.

Figure 8b illustrates the variation of UV-vis spectra concerning Orange II degradation by Co-graphene/PMS system. The two peaks at 310 and 230 nm are attributed to aromatic ring absorptions. The peak at 484 nm is referred to the $n-\pi^*$ transition involving the lone pair on N atoms and the conjugated system extending over the two aromatic moieties and encompassing the N-N group of the hydrazone form.⁴³ The three main absorption bands decreased simultaneously with time and finally disappeared, indicating complete destruction of the azo and naphthalene structure of Orange II.^{44,45} In order to understand the degradation efficiency of Orange II by Co-graphene/PMS system, the effects of

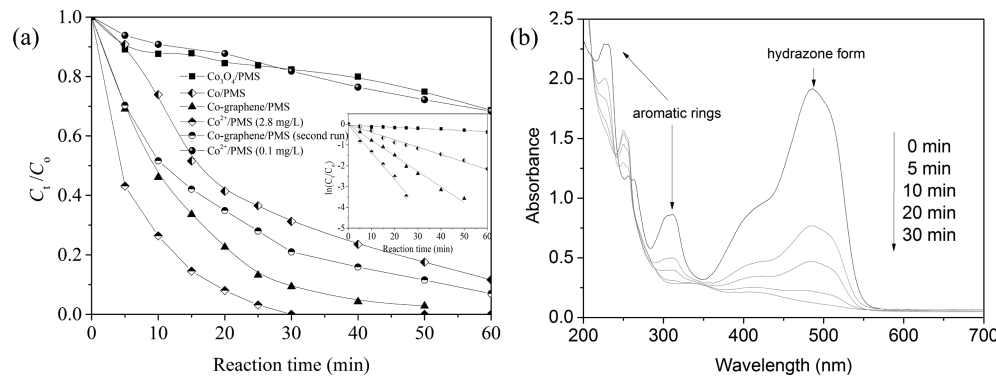


Figure 8. (a) Orange II degradation using different catalysts. (b) UV-vis spectral changes for Orange II degradation with Co-graphene/PMS system. (Reaction conditions: [Orange II] = 60 mg/L, [PMS] = 0.2 g/L, [Co content of Catalyst] = 2.8 mg/L, pH = 7, T = 25 °C).

different operating parameters, including initial solution pH, concentrations of PMS and Orange II, and reaction temperature, were further investigated. As presented in Figure 9, the

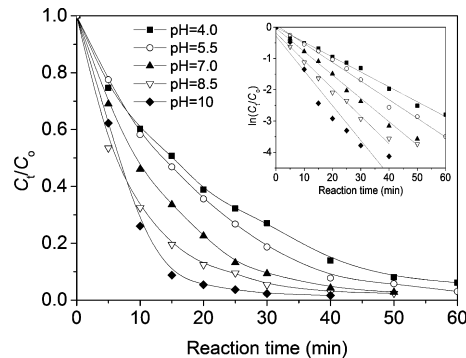


Figure 9. Effect of pH on degradation efficiency by the Co-graphene/PMS system. The inset indicates the kinetics of Orange II degradation. Reaction conditions: [Orange II] = 60 mg/L, [PMS] = 0.2 g/L, [Co-graphene] = 10 mg/L, T = 25 °C.

solution pH can remarkably influence pollutant degradation rate.⁴⁶ At pH 4.0, 94% of Orange II was removed in 60 min, and the Orange II degradation showed significant enhancement with increasing solution pH. The highest catalytic activity was obtained at a pH value of 10 and the rate constant was about 2.3 times more than that at pH 4.0. At the higher pH value, the formation of Co-OH complexes at the surface of Co-graphene was enhanced, which consequently facilitated the heterogeneous PMS activation.⁴⁷ Thus, pH could be taken as an important means to manipulate the degradation of pollutants in the $\text{SO}_4^{\cdot -}$ system.

The effect of initial dye concentration on Orange II degradation on Co-graphene/PMS system was also carried out. Figure 10 demonstrated that an increase in dye concentration from 30 to 120 mg/L resulted in a decrease in reaction rate and dye degradation efficiency. This observation is very similar to the finding in other oxidation systems. A plausible reason might be that, under the conditions of a constant amount of reactive oxygen species ($\text{SO}_4^{\cdot -}$ radicals), the relative amount of free radicals attacking the dye molecules reduces as the amount of dye increases. However, even at a high concentration of Orange II, 120 mg/L, 80% of the dye decolorization was still achieved in 1 h.

Figure 11 presents the degradation of Orange II with the Co-graphene/PMS system at various concentrations of PMS.

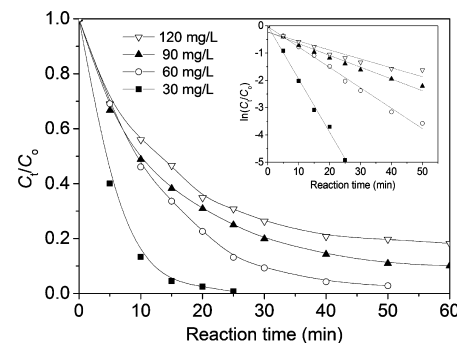


Figure 10. Effect of Orange II concentration on degradation efficiency by the Co-graphene/PMS system. The inset indicates the kinetics of Orange II degradation. Reaction conditions: [PMS] = 0.2 g/L, [Co-graphene] = 0.01 g/L, pH = 7, T = 25 °C.

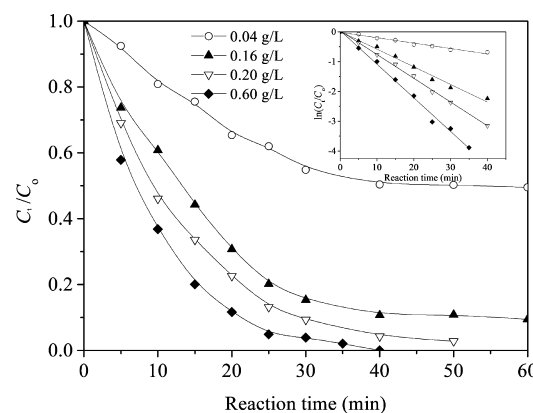


Figure 11. Effect of Oxone concentration on degradation efficiency by the Co-graphene/PMS system. The inset indicates the kinetics of Orange II degradation. Reaction conditions: [Orange II] = 60 mg/L, [Co-graphene] = 0.01 g/L, pH = 7, T = 25 °C.

It can be seen that the Orange II degradation rate greatly increased from $0.018 \text{ to } 0.075 \text{ min}^{-1}$ when PMS concentration increased from 0.04 to 0.20 g/L, which can be attributed to additionally produced $\text{SO}_4^{\cdot -}$ radicals. A further increase in PMS concentration to 0.60 g/L would lead to a slight improvement in dye degradation efficiency. It may be due to the excess of PMS that cannot form a complex with cobalt species contributing to the oxidative degradation of the organic dye. In addition, higher PMS concentration may promote radical scavenging to form $\text{SO}_5^{\cdot -}$ radicals, which have an oxidation potential considerably lower than that of $\cdot\text{OH}$ radicals.

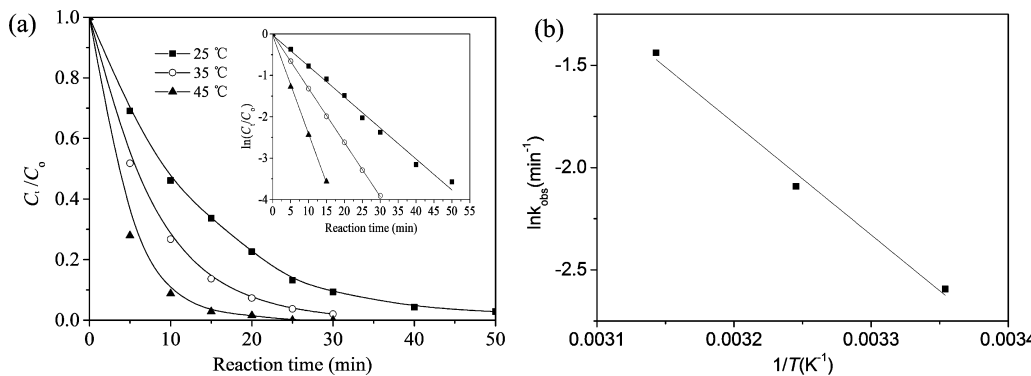


Figure 12. (a) Effect of reaction temperature on degradation efficiency of Co-graphene/PMS system. The inset indicates the kinetics of Orange II degradation versus time. (b) Arrhenius curve. Reaction conditions: [Orange II] = 60 mg/L, [PMS] = 0.2 g/L, [Co-graphene] = 0.01 g/L, pH = 7, T = 25 °C.

Generally, Oxone is dissociated into $\text{SO}_4^{\cdot-}$ either through photolysis or thermolytic cleavage at high temperatures.⁴⁸ Temperature usually has a significant influence on Oxone decomposition rate, which produces $\text{SO}_4^{\cdot-}$. The effect of the temperature on the rate of Orange II degradation by the Co-graphene/PMS system was studied in experiments performed at 25, 35, and 45 °C (see Figure 12a). As it is shown, the removal of Orange II was 90% after 30 min reaction at 25 °C, and a higher reaction rate was observed at 45 °C. The k_{obs} values of Orange II degradation were enhanced with a gradual rise in the temperatures, suggesting that increased temperature could remarkably increase the Orange II removal rate. This is ascribed to the fast Oxone decomposition at high temperatures, which in turn generates more $\text{SO}_4^{\cdot-}$ species than at low temperatures. Oxone could, therefore, be better used as an oxidant at high temperatures.

It is well known that the dependence of the apparent rate constant k_{obs} upon the temperature (T) is usually represented by the Arrhenius equation (eq 1), as shown in Figure 12b

$$\ln(k_{\text{obs}}) = \ln(A) - \frac{E_a}{R} \left(\frac{1}{T} \right) \quad (1)$$

where A is the pre-exponential factor, R is the ideal gas constant, and E_a is the activation energy. The slope of the Arrhenius plot (Figure 12b) for the range of 25–45 °C yielded $E_a = 49.5 \text{ kJ mol}^{-1}$. This parameter corresponds to the overall reaction because k_{obs} was a measure of Orange II depletion. Because the diffusion controlled reactions energy is higher than the activation energy ($10\text{--}13 \text{ kJ mol}^{-1}$), this catalytic reaction is dominated by the rate of intrinsic chemical reactions on the oxide surface rather than the rate of mass transfer.⁴⁹ Previous investigations show that the activation energy of reactions on different heterogeneous catalysts is between 15.8–75.5 kJ mol⁻¹ (e.g., 15.8 kJ mol⁻¹ on CoFe_2O_4 –graphene,²² 26.5 kJ mol⁻¹ on Co_3O_4 –graphene,¹⁷ 61.7–75.5 kJ mol⁻¹ on $\text{Co}_3\text{O}_4/\text{SiO}_2$,⁵⁰ 69.7 kJ mol⁻¹ on $\text{Co}/\text{ZSM}-5$,⁵¹ and 59.7 kJ mol⁻¹ on Co/AC).³ Even though it is unlikely for a comparison of the catalytic activity among various heterogeneous catalysts because of the difference in experimental conditions, the results support that Co-graphene catalyst will be a promising catalytic material for oxidation processes. Table 1 summarizes the results of all experiments.

3.3. Role of Co-Graphene. There were many reports on zerovalent iron (ZVI) in the decontamination of organic pollutants initiated by dissolved oxygen,^{52,53} hydrogen peroxide,⁵⁴ persulfate,⁵⁵ and PMS.⁵⁶ In this work, as an alternative

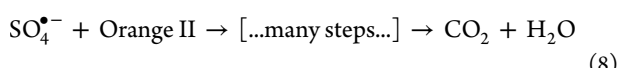
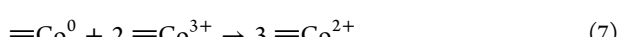
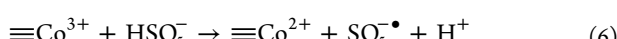
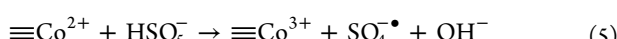
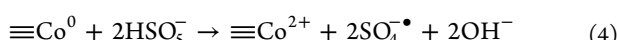
Table 1. Results Summarized for Orange II Degradation

number	variation parameter ^a	k_{obs} (min ⁻¹) ^b	R^2 of k_{obs}	standard error
1	$\text{Co}_3\text{O}_4/\text{PMS}$	0.00501	0.917	5.00×10^{-4}
2	Co/PMS	0.0357	0.984	0.00154
3	Co-graphene/PMS	0.0747	0.992	0.00244
4	$\text{Co}^{2+}/\text{PMS}$	0.131	0.989	0.00627
5	pH = 4.0	0.0477	0.993	0.00133
6	pH = 5.5	0.0597	0.992	0.00183
7	pH = 7.0	0.0747	0.992	0.00244
8	pH = 8.5	0.0885	0.986	0.00376
10	pH = 10	0.111	0.925	0.01194
11	[Orange II] = 30 mg/L	0.195	0.994	0.00662
12	[Orange II] = 60 mg/L	0.0747	0.992	0.00244
13	[Orange II] = 90 mg/L	0.0432	0.968	0.00278
14	[Orange II] = 120 mg/L	0.0326	0.918	0.00343
15	[PMS] = 0.04 g/L	0.0181	0.977	0.00106
16	[PMS] = 0.16 g/L	0.0592	0.985	0.00272
17	[PMS] = 0.20 g/L	0.0747	0.992	0.00244
18	[PMS] = 0.60 g/L	0.113	0.993	0.00370
19	T = 25 °C	0.0747	0.992	0.00244
20	T = 35 °C	0.131	0.999	6.14×10^{-4}
21	T = 45 °C	0.237	0.999	0.00476

^aUnless otherwise stated, the reaction conditions are based on 60 mg/L Orange II, 0.2 g/L PMS, 0.01 g/L Co-graphene, 25 °C, and 60 min degradation. ^b k_{obs} is a pseudo-first-order rate constant.

source to Co^{2+} ion, zerovalent cobalt (eq 2) was employed to activate PMS for the degradation of Orange II. According to previous studies, the primary radical $\text{SO}_4^{\cdot-}$ by Co-graphene/PMS system plays a key role in oxidative degradation of Orange II. Under aerobic conditions, $\equiv\text{Co}^{2+}$ can be released via $\equiv\text{Co}^0$ corrosion. In the process, the release of OH^- upon oxidation of $\equiv\text{Co}^0$ could neutralize the H^+ generated during PMS decomposition. More important, PMS could also directly react with $\equiv\text{Co}^0$ to release $\equiv\text{Co}^{2+}$ in accordance with eq 4. When $\equiv\text{Co}^{2+}$ was generated, it would quickly undergo PMS activation and then produce $\equiv\text{Co}^{3+}$ (eq 5). Some more $\equiv\text{Co}^{2+}$ species are then generated from the reactions between $\equiv\text{Co}^{3+}$ and PMS (eq 6). Thus, $\equiv\text{Co}^{2+}$ exhibits redox cycling in the presence of PMS and produces $\text{SO}_4^{\cdot-}$, similar to iron ions in a Fenton-like reaction.^{49,57} Furthermore, $\equiv\text{Co}^{3+}$ is deposited onto the zerovalent cobalt surface to initiate the release of $\equiv\text{Co}^{2+}$ as presented in eq 7. In this way, Co catalyst makes the reaction proceed cyclically until PMS is completely consumed

at a long enough reaction time. Therefore, the reaction mechanism is proposed as follows:^{7,58–60}



4. CONCLUSION

Magnetic cobalt NPs anchored on graphene sheets were prepared by using a two-step procedure, consisting of code position and thermal treatment, characterized by different techniques, XRD, FTIR, FESEM, TEM, EDS, TGA, XPS, and Raman spectroscopy, and evaluated in the degradation of Orange II from aqueous solutions. TEM and XRD observations indicate that Co NPs at an average size of 29.9 nm anchored on well-exfoliated graphene sheets. The catalytic performance showed that Co-graphene hybrids exhibited higher catalytic activity than pure Co in the degradation of Orange II, attributed to graphene activation of PMS and NPs dispersion. Orange II degradation on Co-graphene/PMS follows the pseudo-first-order kinetics, and activation energy was obtained to be 49.5 kJ/mol. The rate constant of Orange II degradation increases with increasing temperature and Oxone dosage, but it decreases with increasing initial concentration of Orange II. Co-graphene hybrids are, thus, effective catalytic materials for environmental applications.

AUTHOR INFORMATION

Corresponding Authors

*Y. Yao. Phone: +86 551 62901458. Fax: +86 551 62901450. E-mail: yaoyunjin@gmail.com.

*S. Wang. Phone: +61 8 9266 3776. Fax: +61 8 9266 2681. E-mail: shaobin.wang@curtin.edu.au.

Notes

The authors declare no competing financial interest.

ACKNOWLEDGMENTS

The supports by the Anhui Provincial Natural Science Foundation (no. 1308085MB21), the National Natural Science Foundation of China (grant 51372062), the Fundamental Research Funds for the Central Universities (no. 2012HGQC0010), the Technology Foundation for Selected Overseas Chinese Scholar of Anhui Province (no. 2013AHST0415), the Innovative Training Project for Students of Hefei University of Technology (no. 2013CXSY365), and the Project Sponsored by the Scientific Research Foundation for the Returned Overseas Chinese Scholars, State Education Ministry are gratefully acknowledged. The support from Australian Research Council for DP110103699 is also acknowledged.

REFERENCES

- (1) Yang, Z.; Wang, H.; Chen, M.; Luo, M.; Xia, D.; Xu, A.; Zeng, Q. Fast degradation and biodegradability improvement of reactive brilliant red x-3b by the cobalt(II)/bicarbonate/hydrogen peroxide system. *Ind. Eng. Chem. Res.* **2012**, *51*, 11104–11111.
- (2) Yuan, S.; Fan, Y.; Zhang, Y.; Tong, M.; Liao, P. Pd-catalytic in situ generation of H₂O₂ from H₂ and O₂ produced by water electrolysis for the efficient electro-fenton degradation of rhodamine B. *Environ. Sci. Technol.* **2011**, *45*, 8514–8520.
- (3) Shukla, P. R.; Wang, S.; Sun, H.; Ang, H. M.; Tadé, M. Activated carbon supported cobalt catalysts for advanced oxidation of organic contaminants in aqueous solution. *Appl. Catal., B* **2010**, *100*, 529–534.
- (4) Lente, G.; Kalmár, J.; Baranyai, Z.; Kun, A.; Kék, I.; Bajusz, D.; Takács, M.; Veres, L.; Fábián, I. One-versus two-electron oxidation with peroxyomonosulfate ion: Reactions with iron(II), vanadium(IV), halide ions, and photoreaction with cerium(III). *Inorg. Chem.* **2009**, *48*, 1763–1773.
- (5) Chen, X.; Chen, J.; Qiao, X.; Wang, D.; Cai, X. Performance of nano-Co₃O₄/peroxyomonosulfate system: kinetics and mechanism study using Acid Orange 7 as a model compound. *Appl. Catal., B* **2008**, *80*, 116–121.
- (6) Chan, K. H.; Chu, W. Degradation of atrazine by cobalt-mediated activation of peroxyomonosulfate: Different cobalt counteranions in homogenous process and cobalt oxide catalysts in photolytic heterogeneous process. *Water Res.* **2009**, *43*, 2513–2521.
- (7) Yang, Q.; Choi, H.; Al-Abed, S. R.; Dionysiou, D. D. Iron–cobalt mixed oxide nanocatalysts: Heterogeneous peroxyomonosulfate activation, cobalt leaching, and ferromagnetic properties for environmental applications. *Appl. Catal., B* **2009**, *88*, 462–469.
- (8) Lv, A.; Hu, C.; Nie, Y.; Qu, J. Catalytic ozonation of toxic pollutants over magnetic cobalt-doped Fe₃O₄ suspensions. *Appl. Catal., B* **2012**, *117–118*, 246–252.
- (9) de la Peña O’Shea, V. A.; de la Piscina, P. R.; Homs, N.; Aromí, G.; Fierro, J. L. G. Development of Hexagonal Closed-Packed Cobalt Nanoparticles Stable at High Temperature. *Chem. Mater.* **2009**, *21*, 5637–5643.
- (10) Cheng, W.-T.; Cheng, H. W. Synthesis and characterization of cobalt nano-particles through microwave polyol process. *AIChE J.* **2009**, *55*, 1383–1389.
- (11) Duarte, F.; Maldonado-Hódar, F. J.; Madeira, L. M. Influence of the particle size of activated carbons on their performance as Fe supports for developing fenton-like catalysts. *Ind. Eng. Chem. Res.* **2012**, *51*, 9218–9226.
- (12) Li, L.; Zheng, X.; Wang, J.; Sun, Q.; Xu, Q. Solvent-exfoliated and functionalized graphene with assistance of supercritical carbon dioxide. *ACS Sustainable Chem. Eng.* **2013**, *1*, 144–151.
- (13) Yao, Y.; Miao, S.; Liu, S.; Ma, L. P.; Sun, H.; Wang, S. Synthesis, characterization, and adsorption properties of magnetic Fe₃O₄@graphene nanocomposite. *Chem. Eng. J.* **2012**, *184*, 326–332.
- (14) Choi, W.; Lahiri, I.; Seelaboyina, R.; Kang, Y. S. Synthesis of Graphene and Its Applications: A Review. *Crit. Rev. Solid State Mater. Sci.* **2010**, *35*, 52–71.
- (15) Fu, Y.; Chen, H.; Sun, X.; Wang, X. Graphene-supported nickel ferrite: A magnetically separable photocatalyst with high activity under visible light. *AIChE J.* **2012**, *58*, 3298–3305.
- (16) Liang, Y.; Li, Y.; Wang, H.; Zhou, J.; Wang, J.; Regier, T.; Dai, H. Co₃O₄ nanocrystals on graphene as a synergistic catalyst for oxygen reduction reaction. *Nat. Mater.* **2011**, *10*, 780–786.
- (17) Yao, Y.; Yang, Z.; Sun, H.; Wang, S. Hydrothermal synthesis of Co₃O₄-Graphene for heterogeneous activation of peroxyomonosulfate for decomposition of phenol. *Ind. Eng. Chem. Res.* **2012**, *51*, 14958–14965.
- (18) Yao, Y.; Xu, C.; Miao, S.; Sun, H.; Wang, S. One-pot hydrothermal synthesis of Co(OH)₂ nanoflakes on graphene sheets and their fast catalytic oxidation of phenol in liquid phase. *J. Colloid Interface Sci.* **2013**, *402*, 230–236.
- (19) Liang, Y.; Wang, H.; Zhou, J.; Li, Y.; Wang, J.; Regier, T.; Dai, H. Covalent hybrid of spinel manganese–cobalt oxide and graphene as

- advanced oxygen reduction electrocatalysts. *J. Am. Chem. Soc.* **2012**, *134*, 3517–3523.
- (20) Guo, S.; Zhang, S.; Wu, L.; Sun, S. Co/CoO nanoparticles assembled on graphene for electrochemical reduction of oxygen. *Angew. Chem.* **2012**, *124*, 11940–11943.
- (21) Yao, Y.; Miao, S.; Yu, S.; Ma, L. P.; Sun, H.; Wang, S. Fabrication of $\text{Fe}_3\text{O}_4/\text{SiO}_2$ core/shell nanoparticles attached to graphene oxide and its use as an adsorbent. *J. Colloid Interface Sci.* **2012**, *379*, 20–26.
- (22) Yao, Y.; Yang, Z.; Zhang, D.; Peng, W.; Sun, H.; Wang, S. Magnetic CoFe_2O_4 -graphene hybrids: Facile synthesis, characterization and catalytic properties. *Ind. Eng. Chem. Res.* **2012**, *51*, 6044–6051.
- (23) Hartono, T.; Wang, S.; Ma, Q.; Zhu, Z. Layer structured graphite oxide as a novel adsorbent for humic acid removal from aqueous solution. *J. Colloid Interface Sci.* **2009**, *333*, 114–119.
- (24) Bradder, P.; Ling, S. K.; Wang, S.; Liu, S. Dye adsorption on layered graphite oxide. *J. Chem. Eng. Data* **2011**, *56*, 138–141.
- (25) Chandra, V.; Park, J.; Chun, Y.; Lee, J. W.; Hwang, I.-C.; Kim, K. S. Water-dispersible magnetite-reduced graphene oxide composites for arsenic removal. *ACS Nano* **2010**, *4*, 3979–3986.
- (26) Li, B.; Cao, H.; Shao, J.; Li, G.; Qu, M.; Yin, G. Co_3O_4 @graphene composites as anode materials for high-performance lithium ion batteries. *Inorg. Chem.* **2011**, *50*, 1628–1632.
- (27) Chen, Y.; Wang, Q.; Zhu, C.; Gao, P.; Ouyang, Q.; Wang, T.; Ma, Y.; Sun, C. Graphene/porous cobalt nanocomposite and its noticeable electrochemical hydrogen storage ability at room temperature. *J. Mater. Chem.* **2012**, *22*, 5924–5927.
- (28) Fan, Z.; Yan, J.; Zhi, L.; Zhang, Q.; Wei, T.; Feng, J.; Zhang, M.; Qian, W.; Wei, F. A three-dimensional carbon nanotube/graphene sandwich and its application as electrode in supercapacitors. *Adv. Mater.* **2010**, *22*, 3723–3728.
- (29) Jiang, H. G.; Ruhle, M.; Lavernia, E. J. On the applicability of the X-ray diffraction line profile analysis in extracting grain size and microstrain in nanocrystalline materials. *J. Mater. Res.* **1999**, *14*, 549–559.
- (30) Kundu, P.; Nethravathi, C.; Deshpande, P. A.; Rajamathi, M.; Madras, G.; Ravishankar, N. Ultrafast microwave-assisted route to surfactant-free ultrafine Pt nanoparticles on graphene: Synergistic Co-reduction mechanism and high catalytic activity. *Chem. Mater.* **2011**, *23*, 2772–2780.
- (31) Kim, H.; Seo, D.-H.; Kim, S.-W.; Kim, J.; Kang, K. Highly reversible Co_3O_4 /graphene hybrid anode for lithium rechargeable batteries. *Carbon* **2011**, *49*, 326–332.
- (32) Zhang, J.; Jiang, J.; Zhao, X. S. Synthesis and capacitive properties of manganese oxide nanosheets dispersed on functionalized graphene sheets. *J. Phys. Chem. C* **2011**, *115*, 6448–6454.
- (33) Li, X.; Wang, X.; Song, S.; Liu, D.; Zhang, H. Selectively deposited noble metal nanoparticles on Fe_3O_4 /graphene composites: Stable, recyclable, and magnetically separable catalysts. *Chem.—Eur. J.* **2012**, *18*, 7601–7607.
- (34) Wang, D.; Li, Y.; Wang, Q.; Wang, T. Facile synthesis of porous Mn_3O_4 nanocrystal-graphene nanocomposites for electrochemical supercapacitors. *Eur. J. Inorg. Chem.* **2012**, *2012*, 628–635.
- (35) Li, L.; Guo, Z.; Du, A.; Liu, H. Rapid microwave-assisted synthesis of Mn_3O_4 -graphene nanocomposite and its lithium storage properties. *J. Mater. Chem.* **2012**, *22*, 3600–3605.
- (36) Zhang, Q.; Tian, C.; Wu, A.; Tan, T.; Sun, L.; Wang, L.; Fu, H. A facile one-pot route for the controllable growth of small sized and well-dispersed ZnO particles on GO-derived graphene. *J. Mater. Chem.* **2012**, *22*, 11778–11784.
- (37) Shi, L.; Tao, K.; Kawabata, T.; Shimamura, T.; Zhang, X. J.; Tsubaki, N. Surface impregnation combustion method to prepare nanostructured metallic catalysts without further reduction: As-burnt Co/SiO_2 catalysts for Fischer–Tropsch synthesis. *ACS Catal.* **2011**, *1*, 1225–1233.
- (38) Ji, Z.; Shen, X.; Song, Y.; Zhu, G. In situ synthesis of graphene/cobalt nanocomposites and their magnetic properties. *Mater. Sci. Eng., B* **2011**, *176*, 711–715.
- (39) Lee, G.-J.; Manivel, A.; Batalova, V.; Mokrousov, G.; Masten, S.; Wu, J. Mesoporous microsphere of ZnS photocatalysts loaded with CuO or Mn_3O_4 for the visible-light-assisted photocatalytic degradation of orange II dye. *Ind. Eng. Chem. Res.* **2013**, *52*, 11904–11912.
- (40) Riaz, N.; Chong, F. K.; Man, Z. B.; Khan, M. S.; Dutta, B. K. Photodegradation of orange II under visible light using $\text{Cu}-\text{Ni}/\text{TiO}_2$: Influence of Cu:Ni mass composition, preparation, and calcination temperature. *Ind. Eng. Chem. Res.* **2013**, *52*, 4491–4503.
- (41) Chen, X.; Wang, W.; Xiao, H.; Hong, C.; Zhu, F.; Yao, Y.; Xue, Z. Accelerated TiO_2 photocatalytic degradation of Acid Orange 7 under visible light mediated by peroxymonosulfate. *Chem. Eng. J.* **2012**, *193–194*, 290–295.
- (42) Anipsitakis, G. P.; Dionysiou, D. D. Radical generation by the interaction of transition metals with common oxidants. *Environ. Sci. Technol.* **2004**, *38*, 3705–3712.
- (43) Freyria, F. S.; Bonelli, B.; Sethi, R.; Armandi, M.; Belluso, E.; Garrone, E. Reactions of acid orange 7 with iron nanoparticles in aqueous solutions. *J. Phys. Chem. C* **2011**, *115*, 24143–24152.
- (44) Long, X.; Yang, Z.; Wang, H.; Chen, M.; Peng, K.; Zeng, Q.; Xu, A. Selective degradation of orange II with the cobalt(II)-bicarbonate-hydrogen peroxide system. *Ind. Eng. Chem. Res.* **2012**, *51*, 11998–12003.
- (45) Wang, Z. H.; Yuan, R. X.; Guo, Y. G.; Xu, L.; Liu, J. S. Effects of chloride ions on bleaching of azo dyes by Co^{2+} /oxone reagent: Kinetic analysis. *J. Hazard. Mater.* **2011**, *190*, 1083–1087.
- (46) Guan, Y.-H.; Ma, J.; Li, X.-C.; Fang, J.-Y.; Chen, L.-W. Influence of pH on the formation of sulfate and hydroxyl radicals in the UV/peroxymonosulfate system. *Environ. Sci. Technol.* **2011**, *45*, 9308–9314.
- (47) Zhu, Y.; Chen, S.; Quan, X.; Zhang, Y. Cobalt implanted TiO_2 nanocatalyst for heterogeneous activation of peroxymonosulfate. *RSC Advances* **2013**, *520*–525.
- (48) Diaz Kirmsen, E. M.; Martíre, D. O.; Gonzalez, M. n. C.; Rosso, J. A. Degradation of the herbicides clomazone, paraquat, and glyphosate by thermally activated peroxydisulfate. *J. Agric. Food Chem.* **2010**, *58*, 12858–12862.
- (49) Xu, L.; Wang, J. Magnetic nanoscaled $\text{Fe}_3\text{O}_4/\text{CeO}_2$ composite as an efficient Fenton-like heterogeneous catalyst for degradation of 4-chlorophenol. *Environ. Sci. Technol.* **2012**, *46*, 10145–10153.
- (50) Shukla, P.; Sun, H.; Wang, S.; Ang, H. M.; Tadé, M. O. Nanosized $\text{Co}_3\text{O}_4/\text{SiO}_2$ for heterogeneous oxidation of phenolic contaminants in waste water. *Sep. Purif. Technol.* **2011**, *77*, 230–236.
- (51) Shukla, P.; Wang, S.; Singh, K.; Ang, H. M.; Tadé, M. O. Cobalt exchanged zeolites for heterogeneous catalytic oxidation of phenol in the presence of peroxymonosulphate. *Appl. Catal., B* **2010**, *99*, 163–169.
- (52) Kim, D.-h.; Kim, J.; Choi, W. Effect of magnetic field on the zero valent iron induced oxidation reaction. *J. Hazard. Mater.* **2011**, *192*, 928–931.
- (53) Lee, C.; Keenan, C. R.; Sedlak, D. L. Polyoxometalate-enhanced oxidation of organic compounds by nanoparticulate zero-valent iron and ferrous ion in the presence of oxygen. *Environ. Sci. Technol.* **2008**, *42*, 4921–4926.
- (54) Kallel, M.; Belaid, C.; Boussahel, R.; Ksibi, M.; Montiel, A.; Elleuch, B. Olive mill wastewater degradation by Fenton oxidation with zero-valent iron and hydrogen peroxide. *J. Hazard. Mater.* **2009**, *163*, 550–554.
- (55) Kusic, H.; Peternel, I.; Ukić, S.; Koprivanac, N.; Bolanca, T.; Papic, S.; Božić, A. L. Modeling of iron activated persulfate oxidation treating reactive azo dye in water matrix. *Chem. Eng. J.* **2011**, *172*, 109–121.
- (56) Sun, H.; Zhou, G.; Liu, S.; Ang, H. M.; Tadé, M. O.; Wang, S. Nano- Fe^0 encapsulated in microcarbon spheres: Synthesis, characterization, and environmental applications. *ACS Appl. Mater. Interfaces* **2012**, *4*, 6235–6241.
- (57) Heckert, E. G.; Seal, S.; Self, W. T. Fenton-like reaction catalyzed by the rare earth inner transition metal cerium. *Environ. Sci. Technol.* **2008**, *42*, 5014–5019.

- (58) Anipsitakis, G. P.; Dionysiou, D. D.; Gonzalez, M. A. Cobalt-mediated activation of peroxymonosulfate and sulfate radical attack on phenolic compounds. implications of chloride ions. *Environ. Sci. Technol.* **2006**, *40*, 1000–1007.
- (59) Yuan, R.; Ramjaun, S. N.; Wang, Z.; Liu, J. Effects of chloride ion on degradation of Acid Orange 7 by sulfate radical-based advanced oxidation process: Implications for formation of chlorinated aromatic compounds. *J. Hazard. Mater.* **2011**, *196*, 173–179.
- (60) Liang, C.; Guo, Y.-y. Mass transfer and chemical oxidation of naphthalene particles with zerovalent iron activated persulfate. *Environ. Sci. Technol.* **2010**, *44*, 8203–8208.